Learning-Based High-Precision Force Estimation and Compliant Control for Small-Scale Continuum Robot

Pingyu Xiang, Jingyu Zhang, Danying Sun, Ke Qiu, Qin Fang, Xiangyu Mi, Yue Wang, *Member, IEEE*, Rong Xiong, *Senior Member, IEEE*, and Haojian Lu, *Member, IEEE*

***Abstract*— Small-scale continuum robot-assisted minimally invasive surgery has received crucial attention due to its smaller incisions and high dexterity. In medical scenarios such as radiofrequency ablation and nasal/throat swab sampling, monitoring and controlling the forces applied to human tissue can help improve the safety and comfort level of the procedure. However, the tip-sensor-based force detection method can barely be deployed due to the miniature size of the continuum robot; meanwhile, the mechanical modeling-based high-precision force estimation cannot be realized on account of the continuum robots' complex structure with high nonlinear properties. To address the high-precision force estimation challenge for further compliant control during minimally invasive interventions, a learning-based high-precision force estimation method via long short-term memory (LSTM) is proposed in this paper. On this basis, compliance control and high-precision force tracking can be further realized for small-scale continuum robot. The compliance control ensures a smooth and stable transition during the interaction between the robot and the environment, and force tracking can be utilized for maintaining or precisely controlling the force applied to the human tissue. Finally, the contact force sensing and control experiments are carried out on a small-scale continuum robot system prototype, and a demonstration using a human nasal cavity model is conducted. The results validate that the proposed LSTM neural network fits the mechanical model of the continuum robot well with the root mean square error of 3.44mN, and the control method can significantly compensate for the instantaneous impact during contact with an attenuation of 59.3% and rapidly respond to keep the force accurately at the expected value with the mean absolute error of 2.41mN.**

***Note to Practitioners*—This research is motivated by the increasing number of applications for small-scale continuum robot-assisted minimally invasive interventional surgery, such as radiofrequency ablation, biopsy, and endoscopic submucosal dissection. These surgeries require high-precision contact force sensing and control. However, due to the small size and complex structure of the continuum robot, traditional methods such as installing force sensors and mechanical modeling are not effective. Therefore, this paper utilizes a neural network to infer contact force through more accessible information about the robot, such as the tension of the actuators. This method allows for compliant force control during the dynamic contact between the small-scale continuum robot and human tissue. Experiments conducted on a human nasal cavity model demonstrate that the proposed method can improve the safety and reliability of small-scale continuum robot-assisted minimally invasive surgery.**

***Index Terms*— Micro/nano robots, automation at micro-nano scales, small-scale continuum robot.**

I. Introduction

WITH high dexterity, environmental adaptability and safety, small-scale robots have been widely used in minimally invasive surgery (MIS), allowing reach into the human body through flexible access routes while reducing or eliminating incisions. While magnetic-driven microrobots offer similar functions and the potential for reduced size and invasiveness [1], [2], [3], [4], which makes them promising candidates for applications in drug delivery and non-invasive surgery, the requirements for load capacity, real-time force feedback, and enhanced versatility during surgical procedures highlight the important role of small-scale continuum robots in medical treatments. Many surgical applications have demonstrated the capabilities of continuum robot surpassing the conventional rigid robot, such as neurosurgery [5], otolaryngology [6], abdominal surgery [7], vascular surgery [8], etc.

As the broader surgical application, continuum robots are subjected to interact with the anatomy, which makes active compliance and contact force control typically crucial. It can help the system contact the surrounding anatomy smoothly and safely and maintain or precisely control the forces applied to the human tissue [9], [10], [11], which has been shown to be essential for patient safety and enhanced surgery effect [12], [13], [14], [15], [16].

Dupont et al. [17] introduce a hybrid direct force/position control framework initially used for rigid-link robots, where the reference position and force are projected onto the orthogonal subspaces of the configuration space. However, this

Manuscript received 18 July 2023; accepted 26 August 2023. This article was recommended for publication by Associate Editor T. Xu and Editor L. Zhang upon evaluation of the reviewers' comments. This work was supported in part by the Zhejiang Provincial Natural Science Foundation of China under Grant LD22E050007, in part by the Key Research and Development Program of Zhejiang under Grant 2022C01022, in part by the National Natural Science Foundation of China under Grant T2293724, in part by the Fundamental Research Funds for the Zhejiang Provincial Universities under Grant 2021XZZX021, in part by the Science and Technology on Space Intelligent Control Laboratory under Grant 2021-JCJQ-LB-010-13, and in part by the Zhejiang Laboratory under Grant 2020KB0AC02. *(Corresponding author: Haojian Lu.)*

The authors are with the State Key Laboratory of Industrial Control and Technology, and the Institute of Cyber-Systems and Control, Zhejiang University, Hangzhou 310027, China (e-mail: xiang_py@zju.edu.cn; jingyu_zhang@zju.edu.cn; danyingsun@zju.edu.cn; ke.qiu@zju.edu.cn; qinfang@zju.edu.cn; 22232131@zju.edu.cn; wangyue@iipc.zju.edu.cn; rxiong@zju.edu.cn; luhaojian@zju.edu.cn).

Color versions of one or more figures in this article are available at https://doi.org/10.1109/TASE.2023.3311179.

Digital Object Identifier 10.1109/TASE.2023.3311179

framework relies on geometric knowledge of contact and constraints between the robot and the environment, which makes implementing this approach particularly challenging for continuum robots, characterized by high uncertainty in mechanical materials/kinematics, especially when interacting with soft tissues. By leveraging the static model inversion derived in [18], Bajo et al. [19] proposed a new framework for force regulation of multi-segment continuum robots, utilizing the intrinsic actuation sensing of continuum robots. The control accuracy and shape estimation capability are verified on a silicone tissue phantom. In [20], indirect force control is employed, minimizing friction losses in actuation while using an admittance position control loop. This active compliance enables the robot to move robustly in locally unknown environments.

Compared to passive compliance relying on the intrinsic softness of materials, continuum robots with active compliance can exhibit adaptable motions in complex human body cavities, reducing unnecessary contact forces and additional injuries. In [21], a compliant controller with internal sensing capabilities is proposed, providing compliant motions to the robot through robot stiffness definition and external generalized force wrench, without explicit environmental knowledge. In [22], tendon tension is predicted using a recurrent neural network, directly minimizing contact forces in the actuator space, avoiding the need for robot modeling and achieving active compliance. In [23], a model-less hybrid position/force control approach is proposed, utilizing online learning of the changing Jacobian matrix during robot-environment interactions to reduce contact forces when traversing unknown environments.

Obviously, to realize active compliance and force control, the need for force sensing has brought significant challenges to both robot control method and system design for continuum robot. That's why most existing commercial continuum surgical robots are only equipped with visual feedback, and doctors can only estimate the pressure exerted on the patient's tissue subjectively through the deformation of the robot, resulting in extra safety risks. To address this problem, researchers have proposed diverse solutions to endow the force control ability of continuum robots.

The most straightforward approach is integrating force sensors at the tip of the robot to measure the magnitude of the contact force and provide feedback like [22] did. These efforts aim at designing miniature force sensors placed at the distal end of the robot. For example, Seibold et al. [24] developed a force sensor with a diameter of only 10mm and the highest resolution of 0.05N. However, the configuration and calibration of this sensor are kind of complicated. Kim et al. [25] have designed a novel low-cost surgical palpation probe with a miniature six-axis force sensor for minimally invasive surgery. However, the need for minimally invasive surgical compatibility and smaller surgical end-effectors limits its application in extremely confined environments.

Considering the nature of the robot, another kind of work shows the feasibility of estimating the contact force by the information of the robot itself, such as the deformation [26] and actuator information. For example, based on the principle of virtual work and the energy expression of the Euler beam, Goldman et al. [27] obtained the mapping between the generalized external force and the actuation forces. On this basis, they designed an algorithm to provide the robot with excellent compliance in unknown environments. However, this method ignored gravity and friction, probably resulting in linearization and inevitable deviation if friction has a significant influence on specific robots. Rucker et al. [28] approximated the continuum robot as a single Cosserat rod and derived the forces and moments exerted on the robot through nonlinear deflection; Mohsen Mahvash [29] applied the Cosserat principle to obtain an accurate approximation of the coupled statics and kinematics of a continuum robot, realizing the perception of end-force and further the first stiffness control. However, this approach requires external electromagnetic-tracking sensors, which are difficult to achieve high precision. Meanwhile, the need for real-time control will encounter inevitable tradeoffs between model complexity, computational cost and accuracy.

With the development of artificial neural networks, data-driven rather than precise modeling methods have shown great potential in the sensing and control of contact forces in continuum robots, even exceeding the performance of model-based approaches in some scenarios [30], [31], [32]. Donat et al. [32] present an innovative data-driven methodology utilizing deep direct cascade learning (DDCL) to establish a virtual sensor for accurately computing the tip contact force of concentric tube continuum robots. Wu et al. [33] made use of the descriptive knowledge of the tip position and behavior of the catheter, forming a compliance control loop with a long short-term memory (LSTM) neural network, which drives the robot to avoid obstacles automatically and reduces the contact force between the robot and the environment by 70%. Feng et al. [34] proposed a learning-based method to estimate the static contact force (x-y plane) by the tension of the tendon and compared the performance of different artificial neural networks. However, the dynamic interaction between the robot and the environment is not considered. Su et al. [35] proposed a vision-based method to infer robot force based on tissue deformation. However, the vision-based method is limited by computational resources, and the ever-changing environment in the human body makes training rocky, even affecting the network's inference.

Under the above limitations and challenges, in this paper, a learning-based method to achieve compliance control and contact force tracking for a small-scale tendon-driven robot is explored as shown in Fig. 1. With the advantage that neural networks can fit all nonlinear factors theoretically, this method uses the LSTM network to indirectly estimate the tip force of a continuum robot in the case of both non-contact and contact instead of sensors installed at the distal end of the robot. Considering the difficulty of obtaining high-precision vision and absolute position information in invasive surgery, this method also does not need external vision and real-time position information of the robot. Only the sequence of the actuators' state is input into the neural network, and the relative position of the robot tip is calculated by the kinematics model of the continuum robot. Furthermore, the contact between the continuum robot and human tissue is modeled to

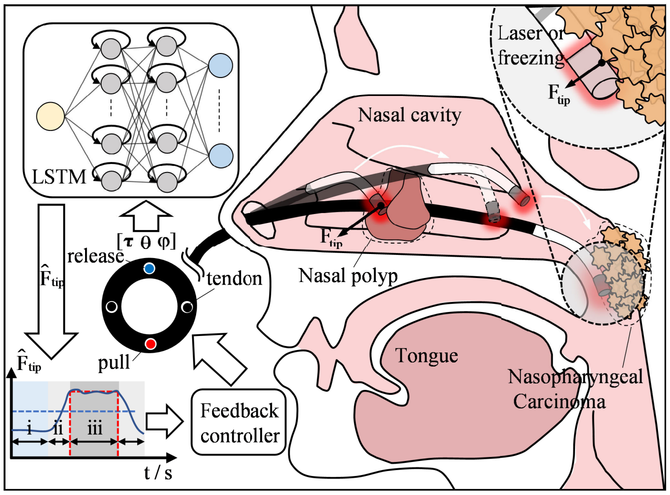

Fig. 1. Principle and application of our learning-based approaches. The proposed method could be used to ablate the nasal polyp and nasopharyngeal for a safer procedure. The plot at the bottom left represents the three stages of the operation process: i) non-contact, ii) contacting, and iii) force tracking.

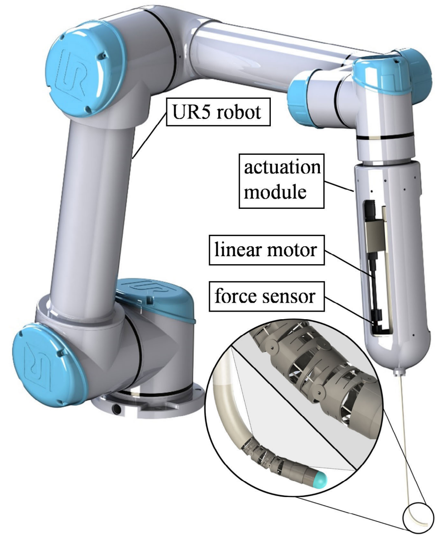

Fig. 2. The medical continuum robot system consists of a UR5 robot, an actuation module equipped with miniature high-precision force sensors and a small-scale continuum robot covered by a waterproof layer.

achieve compliance control and high-precision force tracking. The main contribution of this work includes:

i A learning-based strategy (LSTM) with a simple training procedure is used for estimating the nonlinear mechanical model of the continuum robot, namely the vertical contact force that presses the human tissue.

ii The spring-mass-dashpot model is used to describe the contact between the continuum robot and human tissue to achieve active compliance, and the incremental PID controller is used to track the reference signal with the mean absolute error of 2.41mN.

iii The performance and effectiveness of this method are demonstrated and tested on a small-scale continuum robot system with a human nasal cavity model, where the robot presses on ultra-light clay with similar properties to human tissue to simulate contact with the posterior wall of the human nasopharynx.

The rest of this paper is organized as follows. The robot system and the modelling of the continuum robot are presented and discussed in Section II. Section III details the control methods for robot compliance and force tracking in medical-related scenarios, and the stability analysis is proposed. Then Section IV provides the result and experimental validation of our method. Finally, the conclusion of this study is presented in Section V.

II. Robot System and Modeling

A tendon-driven continuum robot system for MIS is shown in Fig. 2, which consists of three main parts: the actuation module, the continuum robot body and the UR5 robot. The UR5 manipulator is used for installing the actuation module, adjusting the robot to the ideal configuration and providing feed movement in an ample working space so as to slowly feed the continuum robot into the natural cavity of the human. The shell of the actuation module is 3D printed from nylon material, and several linear motors are fixed inside as actuators. Significantly, the connection between the linear motor and the tendon is equipped with miniature force sensors to record the tension when the continuum robot is bent. The continuum robot body consists of two parts. The second half of the continuum robot is a long silica gel hose to increase the effective length of the robot and bend passively, while the first half is a stainless steel multiple interlocked segments made of precision laser cutting, as shown in the enlarged part in Fig. 2. The overall length of the robot is 240mm, with a tip diameter of 3.20mm and a passive bending trunk diameter of 4.58mm. The tendons are attached to the tip of this section and slide in appropriately toleranced holes of the other segments so that the robot can bend in all directions under the drive of the tendons and meanwhile keep tendons parallel. Ablation electrodes or other gripping tools can be attached to the robot's tip for variable applications. In addition, the robot is wrapped in a waterproof material to adapt to the humid environment inside the human body.

In general, the tendon-driven continuum robot can be mainly divided into two parts: the active interventional part at the distal end and the passively bending body when in contact with human tissues. Considering the control ability of the robot, our modelling focuses on the former.

The constant-curvature assumption is a popular and widely-used modelling technique by treating the robot with concatenated constant-curvature arcs [36]. Abundant relevant literature also shows a great performance of the constant-curvature assumption [37], [38]. Thus, we apply the constant-curvature assumption in this work as well.

The contact modelling of a single-segment continuum robot driven by four tendons is shown in Fig. 3. The tendons are equally spaced with a separation angle $\beta = \frac{\pi}{2}$, and a radius, d, from the central axis of the robot. By adjusting the length of four tendons simultaneously, the robot could swing in the workspace determined by kinematics. As the actuators generate a displacement of $\boldsymbol{q} = \left[q_1\ q_2\ q_3\ q_4\right]^{\mathrm{T}}$,

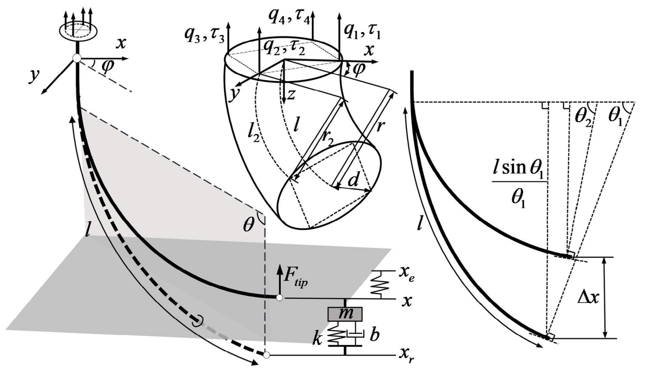

Fig. 3. The modelling of the continuum robot contact with the environment.

actuation force (tensions) on every tendon, denoted by a vector $\boldsymbol{\tau} = \left[\tau_1\ \tau_2\ \tau_3\ \tau_4\right]^{\mathrm{T}}$, will accordingly be produced.

In free space (the dashed line in Fig. 3), a single-segment continuum robot of length l can be described in configuration space as

$$\boldsymbol{\psi} = \left[\,\theta\ \varphi\,\right]^{\mathrm{T}}, \tag{1}$$

where θ and φ represent the bending angle and the angle of the plane containing the robot.

Compared with the forward kinematics, the inverse kinematics of the continuum robot is more commonly used. The mapping between the configuration space and the actuator space is given by the following equation,

$$l_i = l + q_i = l - \theta d \cos\alpha_i, \tag{2}$$

where l_i, $i = 1, 2, 3, 4$, represents the length of the tendons uniformly distributed on the inner surface of the robot, and $\alpha_i = (i-1)\beta - \varphi$. Differentiating (2) yields the differential kinematics of the continuum robot, which associates the differentiation of the configuration space with the differentiation of the actuator space,

$$\dot{q}_i = \left[-d\cos\alpha_i\ \ -\theta d\,\sin\alpha_i\right]\dot{\boldsymbol{\psi}}. \tag{3}$$

According to the mentioned kinematics of the continuum robot, the open loop control with tolerable error in free space can be carried out for the robot after a suitable calibration, which is usually used to adjust the robot configuration in advance to achieve the desired position. However, in practice, the robot's tip is usually in contact with unknown environments. Due to the non-rigidity, it will passively bend by the relative motion direction of the environment, as shown in the solid line to the left of Fig. 3. A contact force F_{tip} will be generated accordingly. Thus, the relation between the displacement caused by environmental contact and robot configuration is considered. This relation can also be applied to the simplified inverse kinematics of the continuum robot from the Cartesian coordinate system to the configuration space, as shown in the right part of Fig. 3. By using Taylor's expansion of the sine function, we get an analytical expression of θ_2, which simplifies subsequent calculations,

$$\Delta x = \frac{l}{\theta_1}\sin\theta_1 - \frac{l}{\theta_2}\sin\theta_2 \approx \frac{l}{\theta_1}(\theta_1 - \frac{\theta_1^3}{6}) - \frac{l}{\theta_2}(\theta_2 - \frac{\theta_2^3}{6}),$$

yielding

$$\theta_2 = \sqrt{6\Delta x/l + \theta_1^2}. \tag{4}$$

In order to model the contact, we simplify the interaction between the robot and environment as a force perpendicular to the plane exerting on the tip, as shown in Fig. 3. In our modelling approach, a user-specified dynamical relationship between the position of the robot's tip x and the contact force F_{tip} is established to add active compliance when contacting. The interaction between the robot and the environment is described as a nonlinear spring-mass-dashpot system,

$$m\frac{\mathrm{d}^2}{\mathrm{d}t^2}(x - x_r) + b\frac{\mathrm{d}}{\mathrm{d}t}(x - x_r) + k(x - x_r) = F_{tip}, \tag{5}$$

where x_r represents the reference trajectory that x should track accurately, and k, b, m are the stiffness coefficients, damping parameters and effective mass, respectively. In many published research [39], [40], [41], it is considered that the contact force F_{tip} is generated by the deformation of $x - x_e$ in the spring-like environment with stiffness k_e and position x_e. Here $x - x_e$ is specified to "penetrate" into the environment. Thus the contact force can be calculated as $F_{tip} = k_e(x - x_e)$ if we know the precise position of the environment x_e and the exact value of the environment stiffness k_e. However, since both the stiffness and location of the environment are challenging to detect or measure, to accomplish force tracking, simply replacing the F_{tip} in Eq. (5) by the tracking error $e = F_r - F_{tip}$ will lead to an undesirable steady error. Here, we only take Eq. (5) as the target impedance for the robot's additional compliance.

III. Method

A. LSTM Neural Network

We aim to take advantage of the data-driven method to get the mapping between the external force and the actuation force of the continuum robot. It must be considered which parameters should be input into the neural network.

According to [21] and [42], the elastic energy of the continuum robot is calculated by the hypothesis of the purely curved beam, and the statics relationship coupled with the robot kinematics is obtained from the principle of virtual work, which is given by the following expression,

$$\mathrm{J}_{\mathrm{q}\boldsymbol{\psi}}^{\mathrm{T}}\boldsymbol{\tau} + \mathrm{J}_{\mathrm{x}\boldsymbol{\psi}}^{\mathrm{T}}\mathbf{F}_e = \nabla\mathbf{E}, \tag{6}$$

where $\mathbf{F}_e$ is the external wrench applied on the continuum robot's tip. $\nabla\mathbf{E}$ is the gradient of elastic energy with respect to a perturbation in configuration space and is related to the material properties of the robot (Young's modulus and moment of inertia) and the instantaneous configuration of the robot. $\mathrm{J}_{\mathrm{q}\boldsymbol{\psi}}$ and $\mathrm{J}_{\mathrm{x}\boldsymbol{\psi}}$ are the Jacobian matrix. Thus, to represent the continuum robot's statics model, it is suggested that the input of the network should include the actuation force and the configuration.

Significantly, in practice, the manufacturing and assembly errors of the robot and the anisotropy of materials make it impossible for continuum robots to be well modeled. More importantly, due to nonlinear friction between the tendon and tube during the movement, the robot has obvious hysteresis

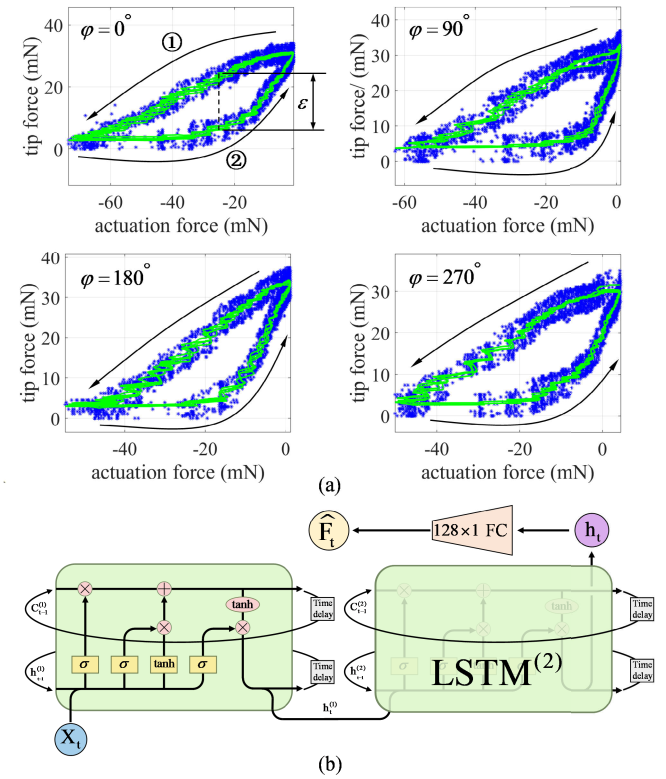

Fig. 4. (a) The relationship between actuation force and contact force when the continuum robot interacts with a fixed environment at different deflection planes; (b) the structure of LSTM-based contact force estimator.

loop properties. As shown in Fig. 4(a), relevant data of four bending planes are recorded during the robot's movement, which intuitively reveals the relationship between actuation force and contact force.

For two different stages of motion (① a bending phase and ② a releasing phase), the same tension can lead to different contact forces with a maximum difference $\varepsilon_{\max}$ of 20mN, about half of the maximum contact force. Even in the same phase, the contact force with previous accumulated errors will fluctuate within a certain range, as shown by the scatter point in Fig. 4(a). Theoretically, a single actuation force corresponds to an infinite number of contact forces. In addition, as shown in the four curves in Fig. 4(a), due to the assembly error and other factors, the statics differs under different deflection angles. Therefore, the contact force is related to not only the current actuation force and configuration but also the information of the robot several steps earlier.

Taking into account the above analysis, the structure of the LSTM neural network [43] for modeling the relationship between the tensions, configuration, and the applied tip force is shown in Fig. 4(b). LSTMs are a type of recurrent neural network (RNN) which is normally used to process sequence information. Derived but different from MLPs, RNN can update the weight of the next step with the current internal state so that the previous input can indirectly affect the current output. As shown in Fig. 4(b), The internal state of each cell in time $t-1$ is taken as the input of time t after a time delay. However, with the growth of the input time series,

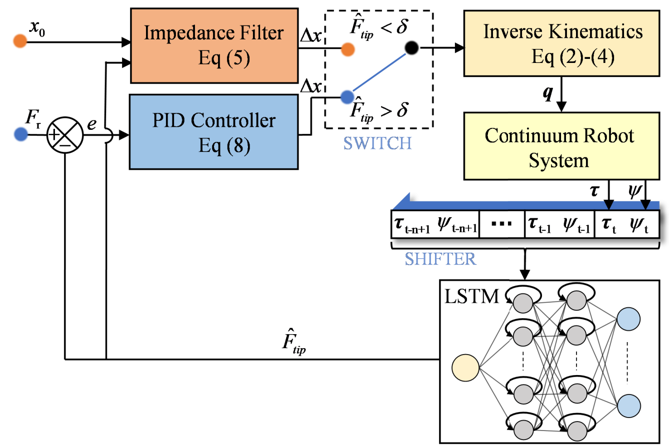

Fig. 5. The control block diagram consisting of an impedance filter and a PID controller, where the switch is flipped according to the contact force estimated by LSTM.

the vanishing gradient problem due to the backpropagation through time still exists in ordinary RNNs [44]. Thanks to the "forget gates", which is denoted by σ at the entry of every cell in Fig. 4(b), LSTM can learn information selectively, without the concern of vanishing gradient, even given millions of discrete time steps. Thus LSTMs much outperform other RNNs in the task of processing time series data, for which it is used to learn the relationship between the tensions, configuration, and the applied tip force here.

We use LSTM with two recurrent layers. The second LSTM takes in the outputs of the first LSTM and computes the LSTM's results. Each recurrent layer has 128 features in the hidden state. To predict the one-DOF contact force $\hat{F}_{tip}$, a fully connected layer (FC) of 128×1 is used to reduce the dimensionality to 1.

B. Compliant Contact and Force Tracking

The control of the robot is divided into three steps, as shown in the curve at the lower left corner of Fig. 1, which are non-contact, contacting and force tracking, respectively.

1) Non-Contact: In free space, the robot has no contact with the environment, $F_{tip} = 0$. At this time, the robot shows various configurations according to the user's requirements to achieve the most appropriate posture for the task. The user can control the robot to reach the desired configuration through direct control instructions or the kinematic mapping of the teleoperation as in [45].

2) Contacting: Once the robot begins to contact the environment, as is presented in Section II, the contact process will be considered a nonlinear spring-mass-dashpot system subjected to external forces. The impedance controller dominates the dynamic response of the robot as in (5). In this paper, we make the damping ratio of the second-order system ξ equals 0.707 and the natural frequency w_n equals 1 in order to obtain better dynamic performance.

3) Force Tracking: Derivation in [39] has shown that if the impedance controller is driven by force tracking error,

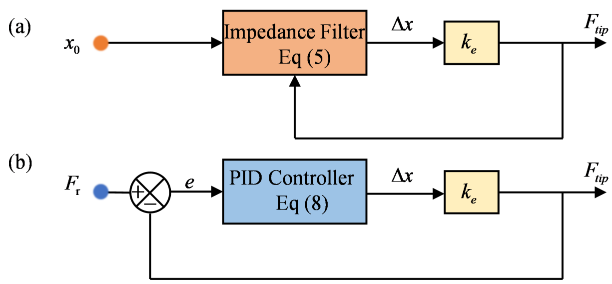

Fig. 6. The two control loops after excluding the neural network.

$e = F_r - F_{tip}$, an undesirable steady-state error,

$$e_{ss} = \frac{kk_e}{k+k_e}(\frac{F_r}{k_e} + x_e - x_r), \tag{7}$$

will occur, where k_e and x_e is time-varying and unknown. This makes the force tracking method based on compliance control intolerable. Thus, we turn to an incremental PID controller for a more reliable effect,

$$\Delta x_{\mathrm{n}} = k_{\mathrm{p}}(e_{\mathrm{n}} - e_{\mathrm{n\text{-}1}}) + k_{\mathrm{i}}e_{\mathrm{n}} + k_{\mathrm{d}}(e_{\mathrm{n}} - 2e_{\mathrm{n\text{-}1}} + e_{\mathrm{n\text{-}2}}), \tag{8}$$

where Δx_{n} is the incremental control command acting on the robot displacement, which can further derive the actuation displacement of the linear motors through Eq. (2)-(4). k_p, k_i, k_d are the proportional, integral, and differential coefficients, respectively. e_n is the tracking error at step n.

In general, as shown in Fig. 1 and Fig. 5, a continuum robot-assistant surgery is summarized into three stages for better therapeutic effect. The first stage is the insertion and posture planning in free space. The second stage is when the robot contacts human tissues with the determined configuration and starts to generate contact force. Corresponding to the orange circuit in Fig. 5, the robot establishes the dynamic relationship between contact force and deformation according to the given physical characteristics. When the contact force reaches a certain threshold δ, the third stage follows. The switch is turned to the blue side. In order to ensure the safety and stability of the operation, the robot maintains the desired contact force in a relatively constant state. Significantly, all of the feedback $\hat{F}_{tip}$ is given by a well-trained LSTM neural network. The LSTM receives the sequence data from a shifter, where the most recent data recorded by sensors is sent to the end of the shifter, and the oldest data is pushed out.

C. Stability Analysis

To ensure the smooth operation and controllability, it is crucial to analyze the stability of the control system. Our proposed method consists of two distinct control loops, which are illustrated separately in Fig. 6 for stability analysis purposes. For the sake of interpretability, we have excluded the estimation process of the neural network from the stability analysis. Instead, we assume that the well-trained LSTM network can effectively substitute the role of the force sensor, accurately estimating the actual contact force within an acceptable margin of error. In the analysis conducted in the second section, we have discussed the relationship between the contact force and the spring-like environment's deformation as,

$$F_{tip} = k_e(x - x_e), \tag{9}$$

where k_e, x, x_e represents the stiffness of the environment, the position of the robot and the environment, respectively.

The impedance filter in Fig. 6(a) is essentially a mass-spring-dashpot model. In this model, when an external force is applied, the position of the system responds compliantly to this force, avoiding rigid collisions. According to Eq. (5), the displacement Δx and the external force F_{tip} can be expressed in the frequency domain by using the Laplace transformation,

$$\Delta x(s) = \frac{F_{tip}}{ms^2 + bs + k}. \tag{10}$$

This is a typical second-order system with all coefficients in the characteristic equation greater than zero. According to the Routh–Hurwitz stability criterion, the system is stable. The choice of damping ratio $\xi = \frac{b}{2\sqrt{mk}}$ determines the transient response. By applying the final value theorem, we can determine the steady state $\Delta x_{ss} = \frac{F_{tip}}{k}$.

In Fig. 6(b), an incremental PID controller is employed, which is the discrete form of a continuous PID controller. The computation result of the incremental PID controller only depends on the most recent three samples of the error, eliminating the need for continuous accumulation. This makes it convenient for implementation in electronic computers. Additionally, by using the control increment as the output of the controller, the potential effects of spurious actions are reduced. Combining it with Eq. (8), the incremental PID controller used in this paper can be represented after the z-transform as

$$x_n(1 - z^{-1}) = [k_p(1 - z^{-1}) + k_i + k_d(1 - 2z^{-1} + z^{-2})]e_n. \tag{11}$$

According to Eq. (11) and the control flowchart in Fig. 6(b), the characteristic equation of the closed-loop pulse transfer function of the system is obtained,

$$N(z) = [1 + k_e(k_p + k_i + k_d)]z^2 - k_e(k_p + 2k_d)z + k_e k_d. \tag{12}$$

According to the Jury stability criterion [46] for discrete systems, under the second-order condition, the sufficient and necessary stability criterion is satisfied, as is verified in Eq. (13), indicating that the discrete closed-loop system is stable.

$$\begin{cases} N(1) = 1 + k_e k_i > 0 \\ N(-1) = 1 + k_e(2k_p + k_i + 4k_d) > 0 \\ a_2 = 1 + k_e(k_p + k_i + k_d) > |a_0| = k_e k_d. \end{cases} \tag{13}$$

IV. Experimental Validation

Several experiments are conducted to verify the validation and performance of the learning-based compliance control and force-tracking method. The experimental setup is shown in Fig. 7. This setup consists of a continuum robot and its actuation module, a UR5 robot, a SRI force sensor module,

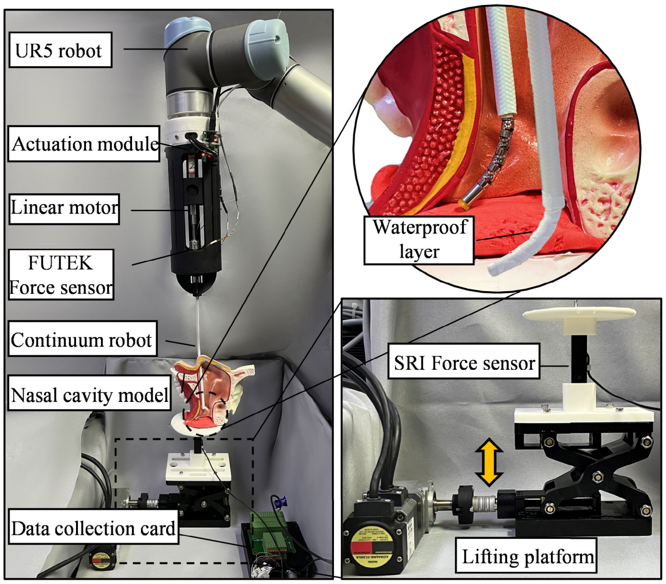

Fig. 7. The experimental setup to collect training data and validate the learning-based control method, which consists of a continuum robot (covered with a waterproof layer) and its actuation module, a UR5 robot, a lifting platform with a SRI force sensor module, an anatomical model of the human nasal cavity, a computer.

a collection unit M8128 for analog-to-digital conversion of the force signal, a lifting platform driven by Oriental Motor, a computer, an anatomical model of the human nasal cavity, and ultralight clay for simulating human soft tissues.

In this setup, the data collected by all sensors is transmitted to the C++ WinForms program running in the Windows operating system via USB serial port. The WinForms program uses UDP to timestamp the collected data and then transmits it to the Python client for visualization, calculation, and inference of the neural network. After testing, the control frequency is about 30-40Hz. The WinForms program directly controls the linear motor actuating the continuum robot, while the UR5 robot is controlled by the WinForms sending instructions to the ROS in the Ubuntu 20.04 virtual machine through the virtual serial port.

A. Training the LSTM Neural Network as Force Sensor

Data for training the network is collected on the experimental platform as shown in Figure 7. In the initial state, there is a certain distance between the robot tip and the lifting platform with a high-precision force sensor. In the robot control process, there is passive bending caused by contact with the environment and operational configuration changes. Thus, the Oriental motor then drives the lifting platform to do reciprocating motion at a certain speed and frequency, simulating the whole process of the robot's contact with the environment. At the same time, the linear motor pulls the tendon, driving the tip of the continuum robot so that it randomly presents different bending angles and bending planes. The experiment system will automatically repeat the process until hundreds of thousands of valid data are collected.

The data acquisition function in our C++ program is activated every 20 ms, resulting in an actual data acquisition

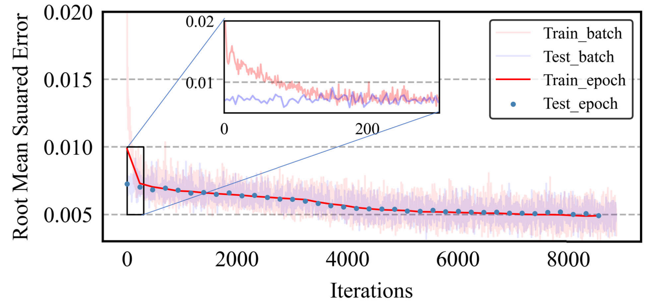

Fig. 8. The training process of LSTM. The part with fast convergence is locally enlarged.

frequency of approximately 50 Hz. Over a sufficient acquisition period, we obtained 171,914 pieces of data with corresponding timestamps without any screening. However, due to the disparity in sampling frequencies between the force sensor on the tendon, the force sensor on the lifting platform, and the C++ program, it is possible that some data may be duplicated or redundant. After eliminating repetitions and minor fluctuations between adjacent data points, we obtained a final set of 117,482 valid data points for further training purposes. To obtain faster convergence speed and training effect, the min-max normalization of each input feature is carried out.

After that, the time series with a length of 20 time steps is obtained by sliding window. The data set was randomly divided into an 80% training set and a 20% test set. The model is implemented in PyTorch and trained by Adam Optimizer with a batch size of 128. During the training, the learning rate gradually decreased from 10^{-3} according to the number of iterations. In order to avoid overfitting and reduce the number of iterations, an early stop is adopted. Once the performance on the test set deteriorates, the training will be stopped, and the optimal network parameters will be saved. The following Fig. 8 shows the convergence of root-mean-square error (RMSE) loss in the training process. After about 6×10^3 iterations, the RMSE decreases to below 5×10^{-3}.

Fig. 9 shows the neural network's performance on the test set. Four fixed period data (about 40 sec) are randomly taken out in the test set and input to the well-trained LSTM neural network to obtain the estimated contact force. The silver lines in the figure represent the robot's bending angles that change randomly during data collection. The result shows that the network performs well on the data set. The RMSE, mean absolute error (MAE), and maximum absolute error (MaxAE) are 1.33mN, 0.94mN and 6.67mN, respectively.

In the follow-up experiments, a real-time force estimating experiment was conducted under different bending planes of the robot to verify the dynamic performance of the network further. The curves in Fig. 10 show the real force and predicted force when the robot comes into contact with a reciprocating platform under different discrete bending planes, φ, from 0° to 315°. It can be found that the network could well estimate the contact force. The results are shown in Fig. 11.

To demonstrate the superiority of the proposed LSTM neural network, we compared it with the classic multi-layer

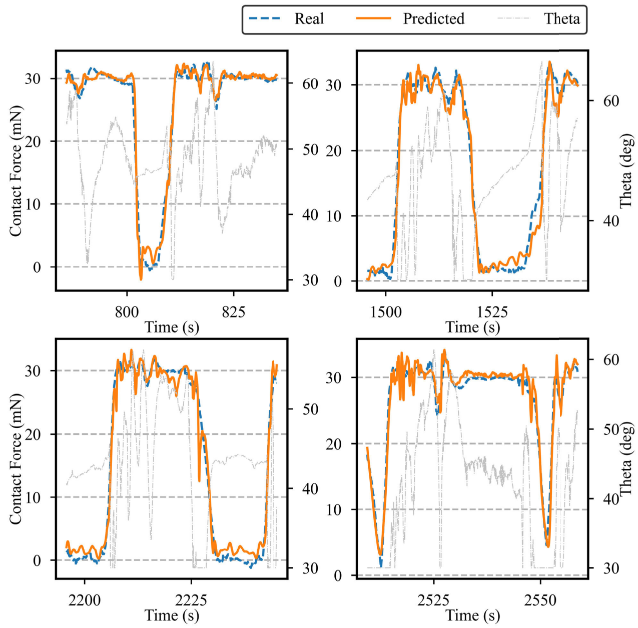

Fig. 9. The performance of the learning-based force estimator when randomly selecting four data sections in the data set and inputting them into the well-trained LSTM.

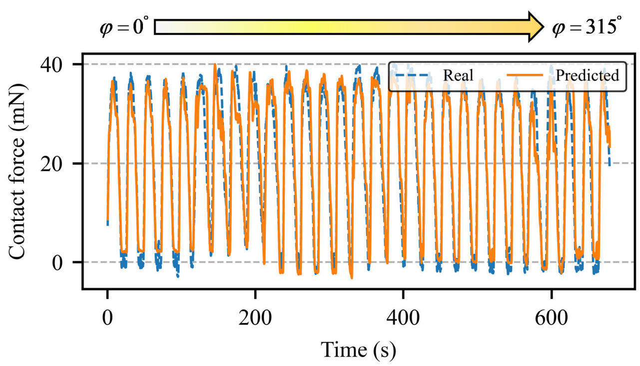

Fig. 10. Real-time force estimation under different bending planes.

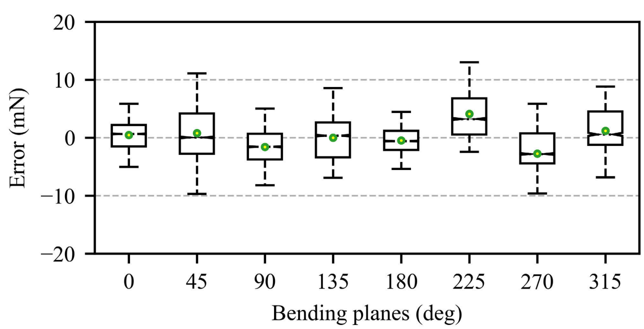

Fig. 11. Force error boxplot of the real-time force estimating under different bending planes.

perceptron (MLP), traditional RNN, and the virtual work model-based (VWM) method described in [21] and Eq. (6) for estimating the contact force of continuum robots. We horizontally compared the performance of these four methods in estimating contact force for small-scale continuum robots, as shown in Fig. 12. The RNN structure we used is similar to LSTM, with only the LSTM cell replaced by RNN units. Additionally, to ensure comparability and persuasiveness, our MLP has two hidden layers with the same number of learnable parameters as the RNN. The learning rate, batch size, loss function, and optimizer hyperparameters were all set to the same values. The models were trained on the same dataset after undergoing the same data preprocessing for the same number of epochs.

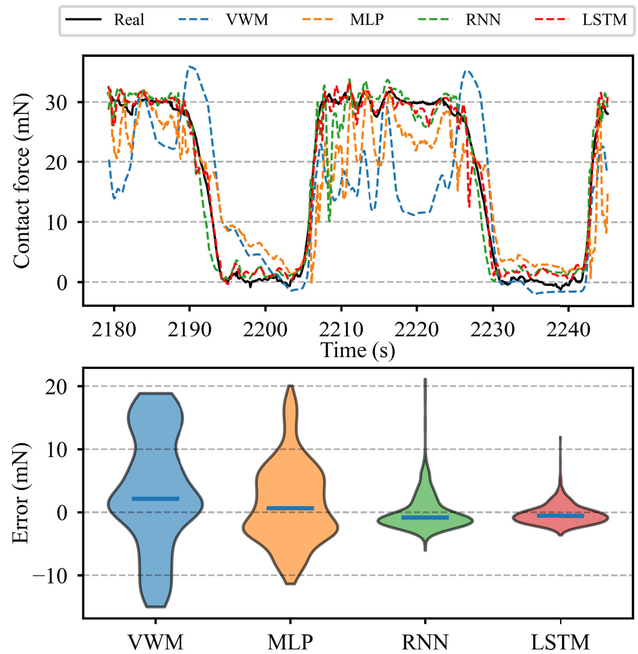

Fig. 12. The performance of contact force estimation utilizing the model-based method, MLP, RNN, and LSTM in one data section, and their error violin plot.

The results of the test set are shown in the first plot of Fig. 12. Overall, the performance of the method based on the virtual work model is the least satisfactory, with an RMSE of 9.61mN. The MLP model performs slightly better with an RMSE of 6.46mN, followed by the RNN model with an RMSE of 2.95mN. The LSTM model exhibits the best performance, achieving the lowest RMSE of 1.70mN.

Analysis of these results reveals that the model-based method neglects many nonlinear factors inherent in the robot itself, which are crucial for accurate estimation in small-scale scenarios. However, it is worth noting that this method paves the way for intrinsic actuation sensing in continuum robots and demonstrates excellent performance in larger-scale continuum robots. The simplicity of the MLP estimator, while not considering sequence dependencies, leads to average performance. The RNN estimator performs just below the LSTM, as it can handle time series data but lacks the robustness of LSTM in processing sequential information. This further validates the need to consider the sequence dependencies in the estimation of contact force for small-scale continuum robots.

B. Compliance and Force Tracking Performance

In order to demonstrate the effectiveness of the compliance control and force tracking method, several experiments are

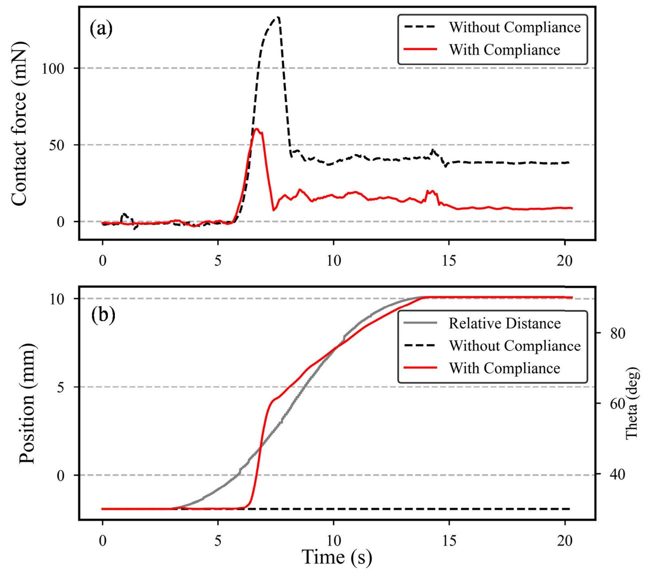

Fig. 13. (a) Contact force with/without active compliance when the robot gradually approaches and contacts the environment. (b) The relative distance between the robot and the environment, and the theta trajectory in both cases.

conducted on the same experimental platform, and the relevant data is recorded.

At first, the tip of the robot is far away from the lifting platform. Then the lifting platform or UR5 robot is driven to move vertically, simulating contact between the robot and the lifting platform. The contact force curve with active compliance and without active compliance is shown in Fig. 13(a). The robot with active compliance can actively change the bending angle, θ of the robot just like a spring-mass-dashpot system during contact (Fig. 13(b)), greatly reducing the impact caused by the instant of contact. Experiments show that active compliance can reduce the maximum impact force of contact from 134.5mN to 54.8mN with an attenuation of 59.3%. It is crucial during surgery, where maximum impact can cause discomfort or injury to the patient, especially in situations such as ablation surgery where contact forces are strictly controlled.

The above compliance loop aims to set a threshold δ for the contacting process. Since the robot does not contact the environment in the free space and does not activate the force tracking loop while changing its configuration to go through the natural cavity of the human. In addition, the operator cannot decide whether the contact is happening in the distance, so a switch shown in Fig. 5 is needed to help the operator determine when the contact has been made and when the contact force needs to be maintained. Moreover, without the absence of the compliance loop, an overshoot exceeding the maximum contact force will be generated due to the instantaneous contact, as the dashed line shown in Fig. 13(a), which is intolerable during the surgical procedure.

In the follow-up experiment, we also test the performance of the force control loop. Incremental PID, in essence, follows the same principles as continuous PID controllers. The proportional, integral, and differential terms have similar adjustment effects. However, incremental PID discretizes the controller using backward difference for computational convenience. It is

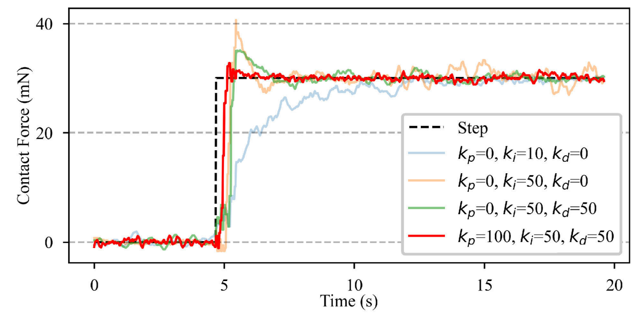

Fig. 14. The acquisition of the proportional, integral, and differential coefficients in the incremental PID controller for high-precision force tracking.

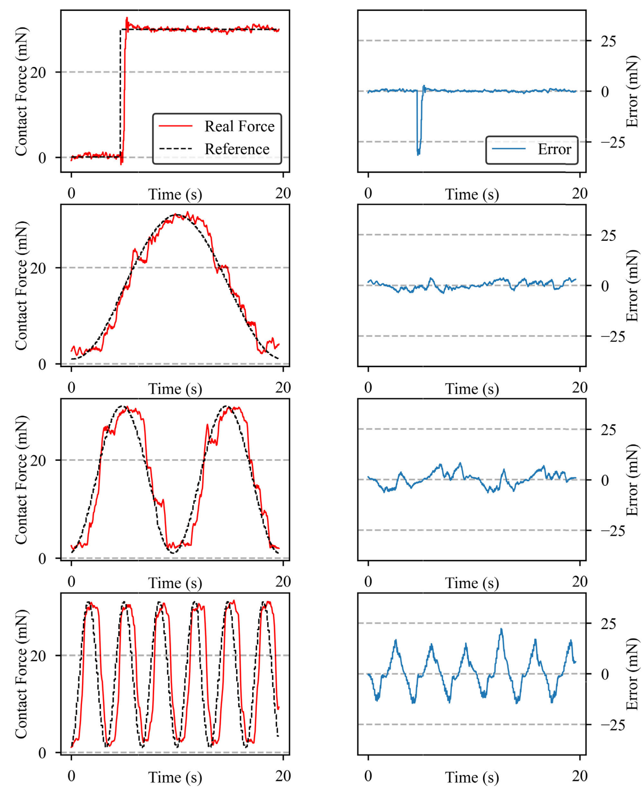

Fig. 15. Force tracking performance and tracking error of the controller under different reference signals (step signal, sinusoidal signal of 0.05Hz, 0.1Hz, 0.3Hz, respectively).

particularly suitable for systems with integral components like stepper motors. In our work, the robot starts from an initial position and adjusts based on the sampled force tracking error, making incremental PID a good choice. Therefore, to achieve better dynamic response, we can tune the coefficients of the incremental PID controller by step response in the time domain. Unlike continuous PID tuning, we typically begin by tuning the k_i coefficient first with k_p and k_d set to 0 to enhance the system's response speed ($k_p = 0$, $k_i = 10$, $k_d = 0$). When the system's response meets expectations, there may be overshoot and oscillations ($k_p = 0$, $k_i = 50$, $k_d = 0$). Increasing k_d helps eliminate oscillations ($k_p = 0$, $k_i = 50$, $k_d = 50$), while increasing k_p reduces overshoot until the desired performance is achieved ($k_p = 100$, $k_i = 50$, $k_d = 50$). The selection of the final coefficients for the PID controller

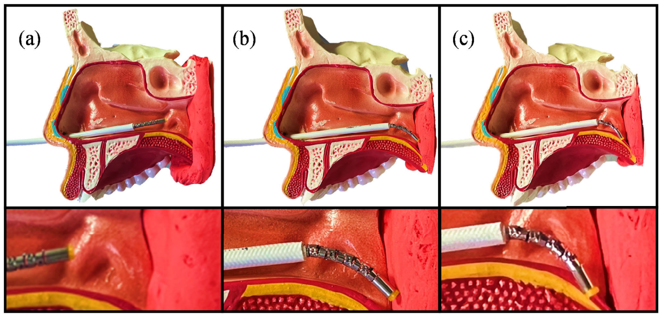

Fig. 16. A complete treatment process on a nasal cavity model, including (a) insertion, (b) contacting and (c) moving away.

is guided by this tuning process. Fig. 14 shows four representative step response curves that demonstrate the coefficient tuning process. The coefficients of the PID controller were ultimately set as $k_p = 100$, $k_i = 100$, $k_d = 50$.

Subsequently, the robot is contacted with the lifting platform to track the step signal with a final value of 30mN and the sinusoidal signal with the amplitude of 30mN and frequency of 0.05Hz, 0.1Hz, 0.3Hz, respectively. As shown in Fig. 15, the signal frequency was chosen with reference to the human respiratory rate in the natural state.

In the step response, the output response enters the error band of 5% of the steady-state within 2.7s, and the steady-state error is closer to 0 with little oscillation. The sudden spike in the error curve is caused by the instantaneous change of the reference signal. It's obvious that the controller could meet the requirement of maintaining constant force in ablation surgery. For low-frequency signals such as 0.05Hz and 0.1Hz, the maximum absolute error of the controller is 4.1mN and 7.7mN, respectively, within the tolerable range. For the high-frequency reference signal of 0.3Hz and above, there is a relatively obvious phase shift of 0.53s, resulting in the maximum absolute tracking error of 22.5mN. With the increase in frequency, the phase shift gradually becomes obvious, which is mainly caused by the phase-frequency characteristics of the controller and the response speed of the hardware. Subsequently, the PID coefficient can be adjusted to cater to the actual respiratory frequency to obtain better performance. The jitter of the control process may come from the sensor's noise and the robot's mechanical characteristics.

C. Experiment on Nasal Cavity Model

Experiments on a human nasal cavity model are carried out to further verify the proposed robotic system's performance and control method. The process can be divided into three steps as shown in Fig. 16. (a) insert into the nasal cavity. (b) compliantly contact the posterior wall of the nasopharynx and maintain a particular contact force. (c) move away from the contact surface. The relative distance between the robot tip and the nasal cavity model is shown in Fig. 17(c). The well-trained LSTM neural network provides force feedback in the progress as shown in Fig. 17(a). We can find out that the magnitude of the contact force can be estimated well using the input of a series of the tendon tension and robot configuration, which is capable of the closed-loop control of

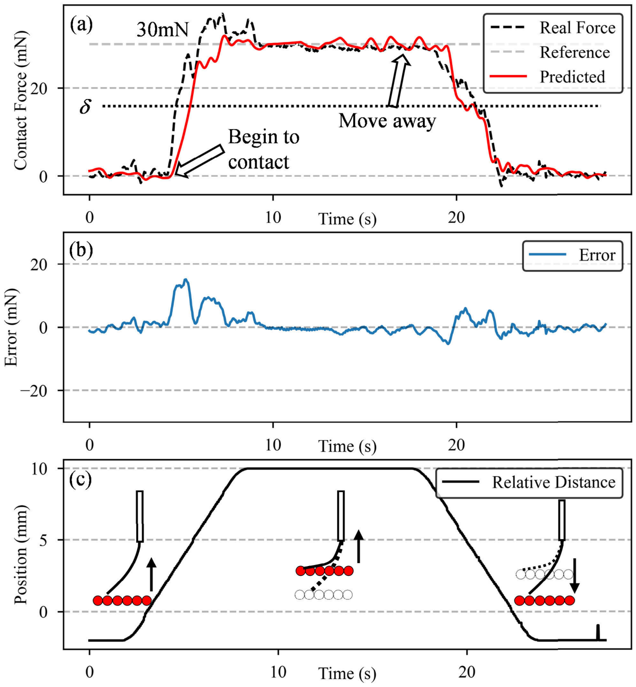

Fig. 17. Performance of the proposed control method during a complete treatment process on a nasal cavity model. (a) Real contact force and predicted contact force. (b) Error of the estimator. (c) Relative distance between the robot and human tissue and its schematics.

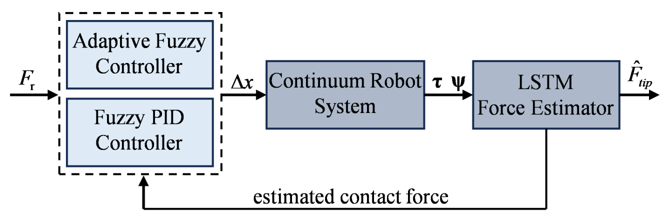

Fig. 18. Control block diagram of adaptive fuzzy controller (AFC) and fuzzy PID controller (FPID) in the continuum robot systems.

the force. And the RMSE, MAE, MaxAE are 3.44mN, 2.07mN and 15.15mN respectively. Significantly, benefiting from the compliance loop, the overshoot of contact force is within 6.91mN.

As for force tracking, it can perform well as long as the force feedback is correct enough. In addition, the program detects the collected data including tendon tension and other information in real-time. If the change is small or there is repetition, the current tensor will not be pushed to the shifter and then input into the LSTM network, which reduces jitter and improves the stability of the system. Therefore, the mean absolute error between the actual and target contact force is as low as 2.41mN.

D. Comparison Results

For comparison purposes, considering the multi-stage task mentioned in the paper, two other robust controllers suitable for this scenario, (i) adaptive fuzzy controller (AFC) and (ii) fuzzy PID controller (FPID), are applied to the small-scale continuum robot system, as shown in Fig. 18. Fuzzy control exhibits robustness to system parameter variations and

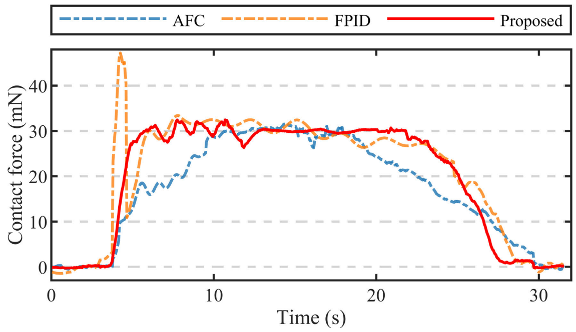

Fig. 19. Performance of the three controllers (AFC, FPID, Proposed) in the comparison experiments on a human nasal model.

environmental uncertainties, and it incorporates expert knowledge into the control process. Due to the highly experiential nature of the entire process of catheter ablation surgery and the absence of a quantitative control objective, two controllers incorporating fuzzy processes are chosen for comparison here.

Firstly, the AFC is given basic expert experience and knowledge, with the fuzzy variables being the estimated contact force and force tracking error and the control information being the change in position of the continuum robot. When defining fuzzy rules, priority is given to achieving the system's compliance, and a variable gain that adapts based on the magnitude of the contact force is designed to improve the system's response performance. The fuzzy PID controller is designed as described in [47]. Both controllers have been appropriately parameterized to achieve a fair comparison.

These two controllers, along with the proposed controller in the paper, are implemented under the same experimental conditions as in the previous section: the nasal cavity model undergoes an up-and-down motion, dynamically coming into contact with the end of the continuum robot. The variation of contact force during the experiment is shown in Fig. 19. The three colored curves represent the response results of the three controllers.

During the ascent phase of the nasal cavity model, when it comes into contact with the robot, the AFC demonstrates excellent compliance and the contact force gradually increases and stabilizes at the target of 30mN after 6.45 seconds. The FPID controller lacks consideration for resisting transient impacts, resulting in a large spike where the contact force reaches 46.86mN momentarily and takes 2.35 seconds to recover from the oscillation, eventually maintaining the force at 30mN. The proposed method, although not as extremely compliant as AFC, is still minimally affected by transient impacts, smoothly moving according to the pre-set compliance while the nasal cavity model is still in the ascending phase, and maintains the force at 30mN after 3.35 seconds. In the subsequent force maintenance phase, the AFC, due to its excessive focus on smoothness, causes the contact force to decrease as the lifting platform descends, maintaining it for less than 10 seconds. On the other hand, both the FPID and our proposed methods can maintain the contact force as long as possible as the platform descends, until the robot completely detaches from the nasal cavity model, with both of them able to sustain the contact force for more than 15 seconds. The MaxAE for force maintenance for AFC, FPID, and the proposed method are 1.58mN, 3.41mN, and 2.46mN, respectively.

The analysis reveals that the design of the fuzzy controller and the formulation of the fuzzy rule base are challenging to obtain a highly optimized and sophisticated performance in such a task. In some specific scenarios, the combination of simple methods (compliance control and PID) can achieve better and more reliable results.

V. Conclusion and Discussion

Robot-assisted minimally invasive surgery deep into the human body has facilitated many new surgical paradigms. This trend urgently requires that the robot operation reach or even exceed the level of conventional surgical instruments. However, force sensing and control, which have been proven vital in most surgeries, are still challenging for small-scale continuum robots. Many researchers have done excellent relative work, and to some extent, they have put forward a good solution for the force sensing and control of the continuum robot. However, for small-scale continuum robots, there is still some inapplicability, such as complex calculation and inconvenient information acquisition.

On the whole, the installation of force sensors at the tip of the continuum robot is strictly limited by the small scale for minimally invasive surgery. Model-based methods to realize end force sensing and compliance control are linearized, and gravity, friction, assembly error and other factors are always neglected. Learning-based methods often require visual or accurate position information, which is difficult to obtain in invasive surgery.

This paper addressed this challenge with a learning-based compliance control and high-precision force control method for a small-scale continuum robot without force sensors integrated at the robot's tip but only through the information at the joint level. Taking advantage of LSTM's ability to process time series data, this method could compensate for the hysteresis caused by assembly errors and internal friction of the tendon-driven continuum robot. After being trained by abundant valid data, the neural network could well fit all the nonlinear features in the static model. In addition, the contact between the continuum robot and the environment is modeled as a spring-mass-dashpot system subject to external force. The relative position is used as the output of the controller, and the corresponding actuation amount is calculated by the kinematics model to achieve compliance control and high-precision force tracking. The experiment conducted on the human nasal cavity model illustrates that this control method can significantly reduce the impact and control the contact force at the desired value with high accuracy.

However, the current work also has some limitations that need further improvement. For instance, the flexible segment at the very end of the robot may be relatively short, resulting in a smaller range for adjusting the force during feeding, still requiring careful handling. In the future, we may address this limitation by installing additional sensors or extending the flexible segment.

We hope that the proposed method can be applied to nasal cavity ablation, cardiac ablation and other scenarios where robots need to penetrate deep into the human body and require strict force control in the future.

REFERENCES

[1] T. Xu, C. Huang, Z. Lai, and X. Wu, "Independent control strategy of multiple magnetic flexible millirobots for position control and path following," *IEEE Trans. Robot.*, vol. 38, no. 5, pp. 2875–2887, Oct. 2022.

[2] T. Xu, Z. Hao, C. Huang, J. Yu, L. Zhang, and X. Wu, "Multimodal locomotion control of needle-like microrobots assembled by ferromagnetic nanoparticles," *IEEE/ASME Trans. Mechatronics*, vol. 27, no. 6, pp. 4327–4338, Dec. 2022.

[3] L. Yang, Z. Yang, M. Zhang, J. Jiang, H. Yang, and L. Zhang, "Optimal parameter design and microrobotic navigation control of parallel-mobile-coil systems," *IEEE Trans. Autom. Sci. Eng.*, early access, Dec. 19, 2022, doi: 10.1109/TASE.2022.3228547.

[4] L. Yang, J. Jiang, X. Gao, Q. Wang, Q. Dou, and L. Zhang, "Autonomous environment-adaptive microrobot swarm navigation enabled by deep learning-based real-time distribution planning," *Nature Mach. Intell.*, vol. 4, no. 5, pp. 480–493, May 2022.

[5] T. A. Mattei, A. H. Rodriguez, D. Sambhara, and E. Mendel, "Current state-of-the-art and future perspectives of robotic technology in neurosurgery," *Neurosurgical Rev.*, vol. 37, no. 3, pp. 357–366, Jul. 2014.

[6] A. Bajo, L. M. Dharamsi, J. L. Netterville, C. G. Garrett, and N. Simaan, "Robotic-assisted micro-surgery of the throat: The trans-nasal approach," in *Proc. IEEE Int. Conf. Robot. Autom.*, May 2013, pp. 232–238.

[7] A. Bajo, R. E. Goldman, L. Wang, D. Fowler, and N. Simaan, "Integration and preliminary evaluation of an insertable robotic effectors platform for single port access surgery," in *Proc. IEEE Int. Conf. Robot. Autom.*, May 2012, pp. 3381–3387.

[8] D. Liu et al., "Magnetically driven soft continuum microrobot for intravascular operations in microscale," *Cyborg Bionic Syst.*, vol. 2022, Jan. 2022, Art. no. 9850832.

[9] J. Tan et al., "A flexible and fully autonomous breast ultrasound scanning system," *IEEE Trans. Autom. Sci. Eng.*, vol. 20, no. 3, pp. 1920–1933, Jul. 2023.

[10] M. Li, X. Qi, Y. Sun, B. Li, Y. Hu, and W. Tian, "A stability and safety control method in robot-assisted decompressive laminectomy considering respiration and deformation of spine," *IEEE Trans. Autom. Sci. Eng.*, vol. 20, no. 1, pp. 258–270, Jan. 2023.

[11] F. Sun, J. Ma, T. Liu, H. Liu, and B. Fang, "Autonomous oropharyngeal-swab robot system for COVID-19 pandemic," *IEEE Trans. Autom. Sci. Eng.*, early access, Sep. 23, 2022, doi: 10.1109/TASE.2022.3207194.

[12] S. B. Kesner and R. D. Howe, "Robotic catheter cardiac ablation combining ultrasound guidance and force control," *Int. J. Robot. Res.*, vol. 33, no. 4, pp. 631–644, Apr. 2014.

[13] A. I. Aviles, S. M. Alsaleh, J. K. Hahn, and A. Casals, "Towards retrieving force feedback in robotic-assisted surgery: A supervised neuro-recurrent-vision approach," *IEEE Trans. Haptics*, vol. 10, no. 3, pp. 431–443, Jul. 2017.

[14] S. Guo et al., "A novel robot-assisted endovascular catheterization system with haptic force feedback," *IEEE Trans. Robot.*, vol. 35, no. 3, pp. 685–696, Jun. 2019.

[15] M. Shurrab et al., "Impact of contact force technology on atrial fibrillation ablation: A meta-analysis," *J. Amer. Heart Assoc.*, vol. 4, no. 9, 2015, Art. no. e002476.

[16] T. Osa, N. Sugita, and M. Mitsuishi, "Online trajectory planning and force control for automation of surgical tasks," *IEEE Trans. Autom. Sci. Eng.*, vol. 15, no. 2, pp. 675–691, Apr. 2018.

[17] P. E. Dupont, N. Simaan, H. Choset, and C. Rucker, "Continuum robots for medical interventions," *Proc. IEEE*, vol. 110, no. 7, pp. 847–870, Jul. 2022.

[18] K. Xu and N. Simaan, "Intrinsic wrench estimation and its performance index for multisegment continuum robots," *IEEE Trans. Robot.*, vol. 26, no. 3, pp. 555–561, Jun. 2010.

[19] A. Bajo and N. Simaan, "Hybrid motion/force control of multi-backbone continuum robots," *Int. J. Robot. Res.*, vol. 35, no. 4, pp. 422–434, Apr. 2016.

[20] R. Yasin and N. Simaan, "Joint-level force sensing for indirect hybrid force/position control of continuum robots with friction," *Int. J. Robot. Res.*, vol. 40, nos. 4–5, pp. 764–781, Apr. 2021.

[21] R. E. Goldman, A. Bajo, and N. Simaan, "Compliant motion control for continuum robots with intrinsic actuation sensing," in *Proc. IEEE Int. Conf. Robot. Autom.*, May 2011, pp. 1126–1132.

[22] D. Jakes, Z. Ge, and L. Wu, "Model-less active compliance for continuum robots using recurrent neural networks," in *Proc. IEEE/RSJ Int. Conf. Intell. Robots Syst. (IROS)*, Nov. 2019, pp. 2167–2173.

[23] M. C. Yip and D. B. Camarillo, "Model-less hybrid position/force control: A minimalist approach for continuum manipulators in unknown, constrained environments," *IEEE Robot. Autom. Lett.*, vol. 1, no. 2, pp. 844–851, Jul. 2016.

[24] U. Seibold, B. Kubler, and G. Hirzinger, "Prototype of instrument for minimally invasive surgery with 6-axis force sensing capability," in *Proc. IEEE Int. Conf. Robot. Autom.*, Apr. 2005, pp. 496–501.

[25] U. Kim, Y. B. Kim, D.-Y. Seok, J. So, and H. R. Choi, "A surgical palpation probe with 6-axis force/torque sensing capability for minimally invasive surgery," *IEEE Trans. Ind. Electron.*, vol. 65, no. 3, pp. 2755–2765, Mar. 2018.

[26] J. So et al., "Shape estimation of soft manipulator using stretchable sensor," *Cyborg Bionic Syst.*, vol. 2021, Jan. 2021, Art. no. 9843894.

[27] R. E. Goldman, A. Bajo, and N. Simaan, "Compliant motion control for multisegment continuum robots with actuation force sensing," *IEEE Trans. Robot.*, vol. 30, no. 4, pp. 890–902, Aug. 2014.

[28] D. C. Rucker and R. J. Webster, "Deflection-based force sensing for continuum robots: A probabilistic approach," in *Proc. IEEE/RSJ Int. Conf. Intell. Robots Syst.*, Sep. 2011, pp. 3764–3769.

[29] M. Mahvash and P. E. Dupont, "Stiffness control of surgical continuum manipulators," *IEEE Trans. Robot.*, vol. 27, no. 2, pp. 334–345, Apr. 2011.

[30] S. Xu, J. Liu, C. Yang, X. Wu, and T. Xu, "A learning-based stable servo control strategy using broad learning system applied for microrobotic control," *IEEE Trans. Cybern.*, vol. 52, no. 12, pp. 13727–13737, Dec. 2022.

[31] K.-H. Lee et al., "Nonparametric online learning control for soft continuum robot: An enabling technique for effective endoscopic navigation," *Soft Robot.*, vol. 4, no. 4, pp. 324–337, Dec. 2017.

[32] H. Donat, S. Lilge, J. Burgner-Kahrs, and J. J. Steil, "Estimating tip contact forces for concentric tube continuum robots based on backbone deflection," *IEEE Trans. Med. Robot. Bionics*, vol. 2, no. 4, pp. 619–630, Nov. 2020.

[33] D. Wu et al., "Deep-learning-based compliant motion control of a pneumatically-driven robotic catheter," *IEEE Robot. Autom. Lett.*, vol. 7, no. 4, pp. 8853–8860, Oct. 2022.

[34] F. Feng, W. Hong, and L. Xie, "A learning-based tip contact force estimation method for tendon-driven continuum manipulator," *Sci. Rep.*, vol. 11, no. 1, Sep. 2021, Art. no. 17482.

[35] Y.-H. Su, K. Huang, and B. Hannaford, "Real-time vision-based surgical tool segmentation with robot kinematics prior," in *Proc. Int. Symp. Med. Robot. (ISMR)*, Mar. 2018, pp. 1–6.

[36] J. Burgner-Kahrs, D. C. Rucker, and H. Choset, "Continuum robots for medical applications: A survey," *IEEE Trans. Robot.*, vol. 31, no. 6, pp. 1261–1280, Dec. 2015.

[37] J. Zhang et al., "A survey on design, actuation, modeling, and control of continuum robot," *Cyborg Bionic Syst.*, vol. 2022, pp. 1–13, Jan. 2022.

[38] R. J. Webster and B. A. Jones, "Design and kinematic modeling of constant curvature continuum robots: A review," *Int. J. Robot. Res.*, vol. 29, no. 13, pp. 1661–1683, Nov. 2010.

[39] H. Seraji and R. Colbaugh, "Force tracking in impedance control," *Int. J. Robot. Res.*, vol. 16, no. 1, pp. 97–117, Feb. 1997.

[40] S. Jung, T. C. Hsia, and R. G. Bonitz, "Force tracking impedance control of robot manipulators under unknown environment," *IEEE Trans. Control Syst. Technol.*, vol. 12, no. 3, pp. 474–483, May 2004.

[41] H. Seraji and R. Colbaugh, "Force tracking in impedance control," in *Proc. IEEE Int. Conf. Robot. Autom. (ICRA)*, May 1993, pp. 499–506.

[42] K. Xu and N. Simaan, "An investigation of the intrinsic force sensing capabilities of continuum robots," *IEEE Trans. Robot.*, vol. 24, no. 3, pp. 576–587, Jun. 2008.

[43] S. Hochreiter and J. Schmidhuber, "Long short-term memory," *Neural Comput.*, vol. 9, no. 8, pp. 1735–1780, Nov. 1997.

[44] R. Pascanu, T. Mikolov, and Y. Bengio, "On the difficulty of training recurrent neural networks," in *Proc. Int. Conf. Mach. Learn. (ICML)*, 2013, pp. 1310–1318.

[45] M. Csencsits, B. A. Jones, W. McMahan, V. Iyengar, and I. D. Walker, "User interfaces for continuum robot arms," in *Proc. IEEE/RSJ Int. Conf. Intell. Robots Syst.*, Aug. 2005, pp. 3123–3130.

[46] E. I. Jury, “A simplified stability criterion for linear discrete systems,” *Proc. IRE*, vol. 50, no. 6, pp. 1493–1500, Jun. 1962.

[47] J. Carvajal, “Fuzzy PID controller: Design, performance evaluation, and stability analysis,” *Inf. Sci.*, vol. 123, nos. 3–4, pp. 249–270, Apr. 2000.

Pingyu Xiang received the B.E. degree in mechatronic engineering from the School of Mechanical Engineering, Zhejiang University, where he is currently pursuing the master’s degree in control science and engineering with the College of Control Science and Engineering, under the supervision of Prof. Lu. His research interests include continuum robotics, medical robotics, and machine learning.

Jingyu Zhang received the M.Eng. degree from the Nanjing University of Science and Technology, Nanjing, Jiangsu, China. He is currently pursuing the Ph.D. degree in robotics with the Soft Medical Robotics Laboratory, Zhejiang University, Hangzhou, China. Previously, he has worked on medical ultrasound scanning system and is currently developing novel different scale of soft continuum to augment the operation ability of surgeons.

Danying Sun received the bachelor’s degree in automation from the Nanjing University of Science and Technology in June 2020. She is currently pursuing the master’s degree with the Robotics Laboratory, Institute of Intelligent System and Control, Zhejiang University. She is supervised by Haojian Lu and her ongoing researching project is magnetic control micronano robot.

Ke Qiu received the B.Eng. degree in mechanical engineering with specialization in mechatronics from the School of Mechanical Engineering, Zhejiang University, China, in 2022, where he is currently pursuing the Ph.D. degree with the College of Control Science and Engineering.

Qin Fang received the master’s degree from the School of Aeronautics and Astronautics, Zhejiang University, where she is currently pursuing the Ph.D. degree with the School of Control Science and Engineering. Her current research interests include the design, fabrication, and control of biomimetic soft robots.

Xiangyu Mi received the bachelor’s degree from the School of Mechanical Engineering, Xi’an Jiaotong University. He is currently pursuing the Graduate degree with the College of Control Science and Engineering, Zhejiang University. He is also working on vision-based tactile sensors, triboelectric, and piezoelectric sensors under the supervision of his advisor, Haojian Lu.

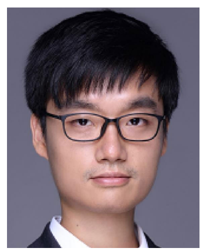

Yue Wang (Member, IEEE) received the Ph.D. degree in control science and engineering from the Department of Control Science and Engineering, Zhejiang University, Hangzhou, China, in 2016. He is currently an Associate Professor with the Department of Control Science and Engineering, Zhejiang University. His current research interests include mobile robotics and robot perception.

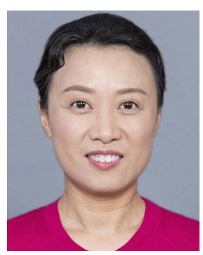

Rong Xiong (Senior Member, IEEE) received the Ph.D. degree in control science and engineering from the Department of Control Science and Engineering, Zhejiang University, Hangzhou, China, in 2009. She is currently a Professor with the Department of Control Science and Engineering, Zhejiang University. Her current research interests include motion planning and SLAM.

Haojian Lu (Member, IEEE) received the B.Eng. degree in mechatronic engineering from the Beijing Institute of Technology in 2015 and the Ph.D. degree in robotics from the City University of Hong Kong in 2019. He is currently a Professor with the State Key Laboratory of Industrial Control and Technology and the Institute of Cyber-Systems and Control, Zhejiang University. His research interests include micro/nanorobotics, bioinspired robotics, medical robotics, micro aerial vehicle, and soft robotics.